

# Is Binary Search Really All You Need? Supercharging Lightweight Database Indexing on GPUs

Justus Henneberg  
Johannes Gutenberg University  
Mainz, Germany  
henneberg@uni-mainz.de

Felix Schuhknecht  
Johannes Gutenberg University  
Mainz, Germany  
schuhknecht@uni-mainz.de

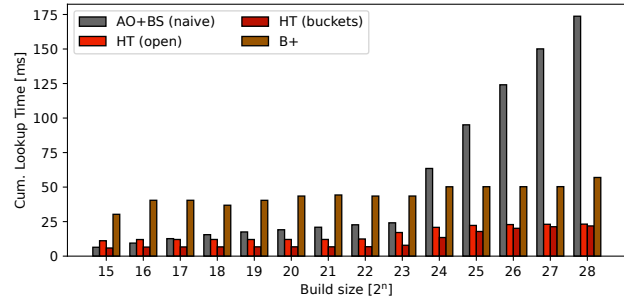
## Abstract

Performing binary search on a sorted dense array is a widely used baseline when benchmarking sophisticated index structures, as it is simple to implement and exhibits a low construction time. However, the popular opinion is that such a simple approach cannot compete with highly-optimized GPU index structures in terms of lookup performance, and hence, should not actually be considered in practice. Interestingly, in our recent works on GPU indexing, we observed a surprisingly good performance of binary search in a variety of situations. Since binary search requires nothing but a sorted array to operate on, which makes it very attractive in the presence of scarce GPU memory, the question arises whether binary search and related variants of it can be made truly competitive and actually replace state-of-the-art index structures, such as a GPU-resident B-Tree and two different hash tables, in read-only scenarios. To find out, as a starting point, we consider five variants of lightweight GPU indexing schemes that offer a minimal or close to minimal memory footprint and analyze how far they are still behind the sophisticated index structures. Step by step, we then “supercharge” them with a set of carefully designed low-level optimizations to incrementally reveal their true potential and the best overall scheme and configuration for answering point lookups and range lookups. Our experimental evaluation reveals that the best optimized lightweight indexes are not only competitive to the sophisticated baselines, but actually manage to outperform them partially while offering a significantly lower memory footprint.

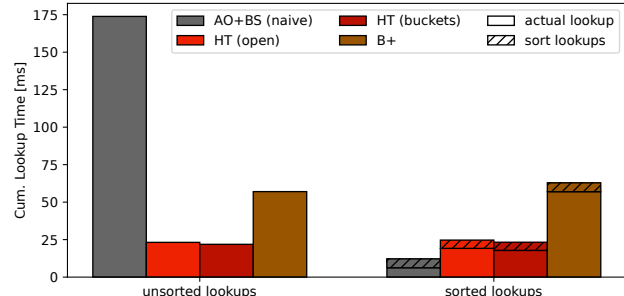
## 1 Introduction

Creating a densely packed sorted array of keys and performing binary search on it can be considered the simplest form of indexing, as its lookup procedure does not rely on any auxiliary data structures. However, despite being used frequently as a baseline in research papers proposing new index structures, the popular opinion is that in terms of performance, it cannot compete with sophisticated indexes, such as B+-trees. While this might be true in the CPU world, we saw a different picture on GPUs in our recent works on GPU-resident index structures. In [14, 15], where we proposed two indexes that are hardware-accelerated using the ray-tracing cores of recent NVIDIA GPUs, binary search on a sorted array performed surprisingly well in certain benchmarks, where it was even outperforming state-of-the-art index structures at times.

The first situation in which binary search on an array in ascending order (called **AO+BS** in the following) performs exceptionally can be seen in Figure 1a, where we show the cumulative lookup time of **AO+BS** in comparison with three other state-of-the-art indexes, namely an open-addressing hash table (**HT (open)**) [17, 19], a bucket-based hash table (**HT (buckets)**) [4] and a B+-Tree (**B+**) [6, 8] while varying the build set size. While



(a) Cumulative lookup time for different build set sizes.



(b) Impact of ordered lookups on the performance.

Figure 1: Situations in which binary search (**AO+BS**) outperforms its traditional competitors.

the performance of all indexes increases when the dataset becomes smaller, **AO+BS** benefits far more than the remaining indexes, even starting to outperform **B+** and **HT** for very small sizes. This nicely demonstrates the core advantage of binary search: With its minimal memory footprint, it can remain fully cache-resident longer than its competitors, which consume more space due to building auxiliary data structures (**B+**) or having to over-allocate memory (**HT (open)**). Further, its code complexity is very low, so each lookup only requires few instructions to be executed. The second situation in which binary search outperforms its competitors can be seen in Figure 1b, where we show the impact of sorting the lookups by their respective search target before performing them. Again, while all indexes benefit from the optimal access locality caused by sorted lookups, **AO+BS** benefits most because of the small number of memory accesses required during a lookup combined with high memory locality, making it significantly faster than all competitors. These results raise the question whether such a simple but memory efficient method as binary search on a sorted array can actually be made competitive in terms of lookup performance in more situations by aligning it closer to the specifics of the underlying

hardware. Achieving this would be exceptionally helpful in environments that (a) have tight space constraints such as entry-tier or older-gen GPUs and (b) have read-only or read-mostly workloads.

To find out, we start with a set of five lightweight GPU indexing schemes that have a minimal or close to minimal memory footprint and see how far they are actually behind the state-of-the-art GPU index structures **B+**, **HT (open)**, and **HT (buckets)**. We then incrementally “supercharge” these lightweight indexes by applying a set of low-level optimizations to improve their point lookup and range lookup performance as far as possible. We consider the following five methods: **(M1) AO+BS**: A (key, row ID)-array where the keys are sorted in ascending order (**AO**) on which an offset-based back-to-front binary search (**BS**) is performed. It has a minimal memory footprint and can be considered the simplest variant. **(M2) EO+BS**: A (key, row ID)-array that is materialized in the so-called Eytzinger order (**EO**), where entries are not sorted in ascending key order, but with respect to the order of potential accesses during search. This potentially offers a better lookup performance due to the increased access locality, but also complicates the correct handling of range lookups. Naturally, this variant also has a minimal memory footprint as it also materializes nothing but a flat dense array. **(M3) AO+PB+BS**: Under relaxed space constraints, we can also materialize the pivot entries accessed during binary search (**BS**) in an *auxiliary* dense pivot buffer (**PB**) serving as a lightweight index layer, which then points to the full (key, row ID)-array ordered by key (**AO**) representing the leaf level. This indexing scheme potentially benefits from fewer cache lines being accessed during traversal just like the Eytzinger order, while preserving the the benefits of a sorted array to ensure efficient range lookups. **(M4) EO+KS** and **(M5) AO+PB+KS**: Of course, instead of using only binary search, we can generalize any of the variants **(M1)**, **(M2)**, and **(M3)** to a  $K$ -ary search (**KS**) for  $K \geq 2$  to support higher search fan-outs. While a larger choice of  $K$  negatively impacts the performance of variant **(M1)** as empirically evaluated, it is worth considering for **(M2)** and **(M3)** as it allows adjusting the height of the search tree and offers a natural way to parallelize the search across  $K-1$  threads. Apart from describing these methods in all detail in Section 3, we formalize a highly efficient and scalable algorithm for building all of the proposed indexing schemes concurrently on a GPU.

To get the most out of these lightweight methods, we **(O1)** carefully investigate the impact of different possible **scheduling strategies** to identify which combination leads to the best resource utilization on the hardware. At the same time, we **(O2)** improve the effectiveness of the L1 cache by introducing **cache pinning** of the upper levels of the search path while **(O3)** increasing the locality of lookups on neighboring hardware threads via the **local reordering** of lookup batches. Further, we **(O4)** identify the best **memory layout** for each method. **(O5)** We test whether the pivot buffer can be trimmed to save space without sacrificing performance. Finally, **(O6)** we inspect the specific needs of answering **range lookups** efficiently and propose separate configurations for this case.

The paper is structured as follows: In Section 2, we first describe the characteristics of the hardware architecture and all necessary background information. In Section 3, we then describe the five methods that serve as our starting point in all detail along with their build mechanism. In Section 4, we next present all potential optimizations, which we then evaluate on our methods in Section 5

to identify the best configuration. In Section 6, we finally compare our best lightweight indexes against the baseline indexes in terms of point and range lookup performance, as well as build time and memory footprint. After discussing the related work in Section 7, we conclude in Section 8.

## 2 Hardware Architecture and Background

Before diving into the methods, let us discuss the architecture and specifics of the underlying hardware. As main testbed, we use an NVIDIA RTX 4090 (Ada architecture), a high-end consumer GPU. The architecture is visualized in Figure 2. Processing on the 4090 is distributed across 128 *streaming multiprocessors* (SMs) containing 4 vector units of 32 cores each. Typically, one unit of work is assigned to one thread. When running a task, the GPU distributes small batches of threads (called *thread blocks*) across SMs, which then schedule even smaller batches of 32 threads (called *warps*) onto the 32-core vector units. Each SM has its own shared L1 cache (128 KB), which can be partially (up to 100 KB) reconfigured to serve as fast user-programmable scratch memory, allowing for fast data movement and storage within a thread block. Similarly, each SM contains 256 KB worth of 32-bit registers, which can be cross-referenced by threads within a warp to exchange data on-the-fly (called *warp shuffling*). Additionally, the GPU has a global L2 cache (72 MB). To ensure scalability, NVIDIA restricts direct communication across SMs, only allowing indirect communication through the GPU’s globally-accessible main memory. Similar to block storage devices, loading larger contiguous chunks (called *coalescing*) from main memory is more efficient than small random accesses. Consequently, memory throughput is maximized if neighboring threads in a warp access neighboring memory addresses. We will show experimental evidence for this in Section 3.4.

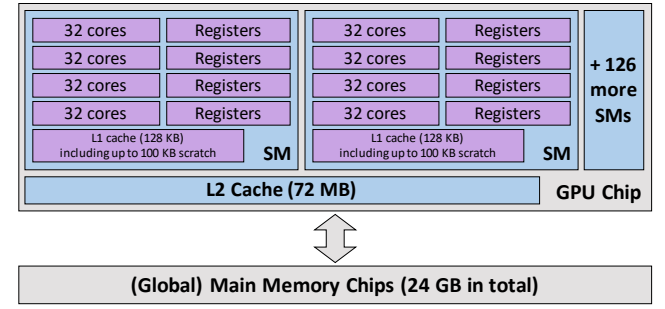


Figure 2: Architecture of the NVIDIA RTX 4090.

## 3 Lightweight Indexing Methods

We begin by describing the lightweight indexing methods we consider as starting points for our study. We further propose an efficient and scalable construction mechanism to build these indexes concurrently on the GPU. After evaluating their current performance, in Section 4, we will then incrementally apply a set of carefully tuned low-level optimizations to see how far we can push these methods.

### 3.1 Ascending Key Order + Binary Search (AO+BS)

Naturally, we first consider the simplest lightweight indexing variant, which traverses an array of size  $n$  that is sorted in ascending order (**AO**) via binary search (**BS**) from the last entry to the first entry using incrementally smaller steps. Initially, the step width

is chosen as the largest power of two that is not greater than  $n$ , which can be determined efficiently using a count-leading-zeros instruction (LPOW2( $n$ )). Given a key to search for, we can perform a step safely if the entry at the stepped-onto position is not smaller than the search key. When the search terminates, offset will point to the first entry not smaller than the key. Since the step width is halved in each iteration, we only require  $\log_2(n)$  many array accesses to locate the key.

Storing keys in ascending order also makes range queries trivial: We can locate the smallest qualifying entry in the buffer using this exact variant of binary search, and then just iterate over the subsequent array entries until we exceed the upper limit.

```

1  def bs(sorted_keys, offset, step, lookup):
2      while step > 0:
3          if step <= offset:
4              if sorted_keys[offset - step] >= lookup:
5                  offset -= step
6          step >>= 1
7      return offset
8
9  kernel naive(sorted_keys, lookups, results):
10     lookup = lookups[TID]
11     offset = len(sorted_keys) - 1
12     step = LPOW2(len(sorted_keys))
13     results[TID] = bs(sorted_keys, offset, step, lookup)

```

**Listing 1: Pseudo-code of the binary search kernel operating on an AO-array.**

Listing 1 shows the pseudo-code for our batch-lookup GPU implementation: Each thread (identified by an integer  $TID$ ) loads a single key for lookup, then performs the binary search, and then stores the result in a separate buffer. Figure 3 visualizes the possible search paths for an example dataset with  $n = 14$  entries. The number below each entry corresponds to the number of search steps after which the element is first visited.

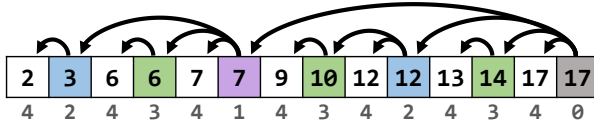


**Figure 3: Search paths of AO+BS.**

### 3.2 Eytzinger Order + Binary Search (EO+BS)

An obvious downside of binary searching through an array that is sorted in ascending order is the occurrence of frequent cache misses due to poor access locality. A solution to this problem is to rearrange the keys so that the entries accessed during step  $i$  of a traditional left-or-right binary search are stored as one contiguous chunk. The pivot elements can be chosen so that the resulting binary search tree is complete, i.e., all levels contain the maximum number of nodes, except for the leaf level, where the existing nodes have to be left-aligned. Because of this, we can represent the resulting tree as a dense array with implicit parent-child relations, similar to a binary heap. This dense tree representation is generally referred to as *Eytzinger order* (EO) [20]. We will present the exact build algorithm in Section 3.5. Since we are still talking about database indexes, along with the keys, we also simultaneously reorder the

associated row ID references, which are not shown in the figures for space reasons.

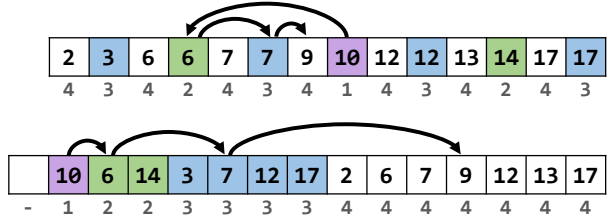


**Figure 4: Performing a point lookup for key 9 using EO+BS (bottom) and its equivalent in an ascending array (top).**

Figure 4 shows an example. The top part of the figure shows the access paths of the traditional left-or-right binary search on our example key set. The bottom part shows the same keys rearranged into Eytzinger order. Note that there is an extra empty slot at the beginning, as this results in better cache alignment. The arrows indicate the steps taken to locate key 9.

EO has one important drawback: Range lookups and key duplicates are more difficult to handle since neighboring keys are no longer stored consecutively. While both occur frequently in real workloads, we did not find any literature discussing these special cases, which is why we now present our own range lookup algorithm. If we want to find all occurrences of a duplicate key  $k$ , we can apply the same algorithm to the range  $[k, k]$ .

Figure 5 shows an example for answering the range lookup  $[9, 12]$  on our usual key set in Eytzinger order (bottom part of the figure). While the qualifying entries no longer form a single coherent chunk, they are at least consecutive within each Eytzinger level, so that a range lookup can be performed by a series of scans. The figure also shows that on each level, the start of this chunk of consecutive qualifying entries coincides with the search path we would take to look up the range query's lower bound.

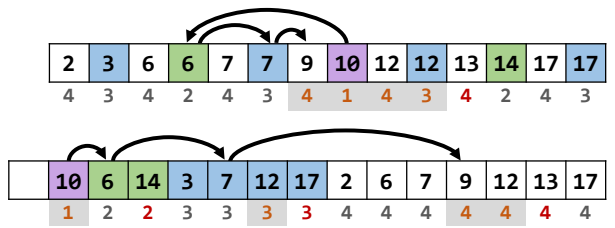


**Figure 5: Performing the range lookup  $[9, 12]$  using EO+BS (bottom) and its equivalent in ascending order (top). Shaded orange indices mark the qualifying entries, while red indices mark entries that do not qualify, but still have to be scanned.**

We demonstrate this strategy using the example in Figure 5: On the root level, we find key 10 which is contained in  $[9, 12]$  and hence becomes a result. The search for the lower bound 9 now continues with the left child, which is 6. Even though 6 itself does not qualify for our query, the array entries directly to the right must be larger than 10 due to the search tree property, so we start our scan at the next position in the array. We continue until we reach the end of the

level, or until we find the first element exceeding the upper bound, which is 14 in our case. Since 6 is strictly smaller than our lower bound 9, we can safely ignore the left subtree and continue with the right child, which is 7. We alternate between scanning a level and switching to the next level until we reach the leaf layer. Note that this implementation only visits up to two additional entries per level apart from the entries that are actually part of the range, which quickly becomes negligible as the size of the query range increases, resulting in minimal overhead.

### 3.3 Ascending Key Order + Pivot Buffer + Binary Search (AO+PB+BS)

Depending on the application, it might still be beneficial that the index maintains all keys in ascending order.

Hence, we consider an alternative that follows the motivation of the Eytzinger order, namely to improve the access locality, but preserves the sorting order at the same time. The core idea is to relax the space constraint a bit and to materialize the pivots that would be traversed during binary search in a separate pivot buffer (**PB**) in GPU memory, while retaining the original array as the leaf layer. By building the implicit tree bottom-up with fixed chunk sizes, we do not need to store child pointers, resulting in minimal memory overhead caused by this auxiliary structure. This design has some similarities to cache-sensitive search trees [25].

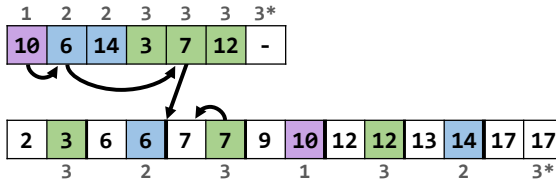


Figure 6: Performing a point lookup for key 7 in AO+PB+BS, using a separate buffer that materializes the pivots. The last key 17 (marked by a star) does not have a partition to the right of it, thus it is not a pivot, and all searches automatically continue traversal to the left.

Figure 6 shows how the data structures look like for our example key set, where the arrows visualize the access path for a point lookup of key 7. As we can see, the first three accesses happen through the pivot buffer, from which we are directed to a fixed-size chunk in the ascending array, which contains the sought-after key.

In contrast to **EO**, all paths in the pivot tree from the root to the leaves have identical lengths, as this reduces instruction divergence during traversal. In exchange, some inner nodes in the pivot buffer might be missing a right child and require special handling, which can only happen at the leaf level in **EO**.

### 3.4 Generalizing Binary Search to $K$ -ary Search

So far, we have only considered variants of *binary* search. However, for all previously discussed options, it is possible to generalize them to a  $K$ -ary search (**KS**) for  $K \geq 2$ . This generalization does not only allow us to configure the tradeoff between the height of the search tree and the width of tree nodes, but offers more flexibility regarding lookup parallelization: For the binary search variants, each lookup can only be performed by exactly one thread and thus,

the parallelism of the hardware can only be utilized properly by executing a large number of lookups in parallel. However, since these lookups are completely independent from each other, adjacent threads likely take diverging paths through the data structure, reducing memory efficiency. Fortunately, by generalizing the approaches to  $K$ -ary search, we are able to naturally distribute a *single* lookup over multiple adjacent threads, which highly improves the access locality.

A traditional binary search would be generalized as follows:  $K$ -ary search recursively selects  $K - 1$  pivot entries at evenly spaced positions, thus partitioning the array into  $K$  chunks, and decides which chunk to search next based on how the lookup key compares to the pivots, similar to how a B-Tree decides which child node to visit next. This comparison step can be performed by  $K - 1$  threads in parallel, after which all threads communicate their results to figure out which partition to search next. For small  $K$ , this communication step can be done efficiently using warp shuffles.

Generalizing the naive variant **AO+BS** to **AO+KS** would result in  $K - 1$  expensive random accesses when accessing the pivots due to their relative spacing, which is highly inefficient. However, **EO+KS** and **AO+PB+KS** provide the opportunity to store the pivots in neighboring slots, which makes us expect better performance from the increase in access locality.

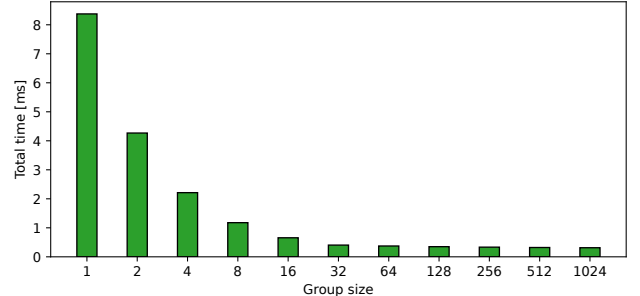


Figure 7: Quantifying the benefit of coalesced memory loads.

To support this claim, we ran the following micro-benchmark: We allocate an array with  $2^{28}$  32-bit entries and fill it with random values. We then spawn a total of  $2^m$  threads, where  $2^m$  neighboring threads form a group (resulting in  $2^{16-m}$  disjoint groups). Each group then performs 1024 lookup steps. In each step, each group draws a random position  $p$  within the array to load from, simulating diverging access paths for far-spaced accesses. Meanwhile, within a group, thread  $i$  loads from position  $p + i$ , so that the group loads  $2^m$  entries in total, and neighboring threads access neighboring entries. Note that the total amount of load operations remains constant, only their pattern changes. We plot the execution time of the lookup steps for various group sizes in Figure 7. The figure shows a 50% decrease in execution time each time we double the group size, up to 16. Moving to group size 32 yields a smaller benefit, and any increase beyond 32 does not result in faster execution. In other words, a coalesced load of 16 entries costs the same as loading a single entry.

We utilize this for **AO+PB+KS**, which generalizes the pivot buffer. It operates as shown in Figure 8 for  $K = 3$ , where 7 and 14

are chosen as the  $K - 1 = 2$  pivots for the first step, and 3/6 or 10/12 are materialized as the pivots for the second step. To perform a lookup of key 13, two threads are now able to concurrently load and compare the pivots 7 and 14 with the search key 13. As 7 is smaller than 13 while 14 is not, the threads can exchange this information to continue the search in the middle (second) chunk on the next level. We repeat this procedure until we are finally directed to a chunk in the sorted array, the one containing 13. Note that thread grouping also improves range lookups: We can first locate the smallest qualifying entry as described above, then re-use our group of adjacent threads to load multiple subsequent entries at once and process them simultaneously, resulting in even more coalesced memory accesses.

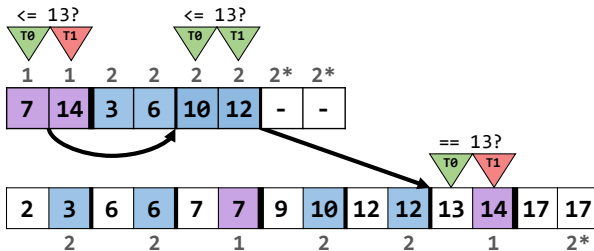


Figure 8: Point lookup of key 13 for AO+PB+KS.

The variant **EO+KS**, which generalizes the Eytzinger order, looks and operates as visualized in Figure 9, where we show a point lookup of key 13 for  $K = 3$ . As a consequence, on each level of the search tree, two elements can now be compared by two threads in parallel. In contrast to the **PB** variants, **EO** does not have to traverse the tree all the way to the bottom if we find a key in an inner node. This is because **EO** stores the row IDs along with the keys, whereas the pivot buffer contains keys only and therefore has to be traversed entirely.

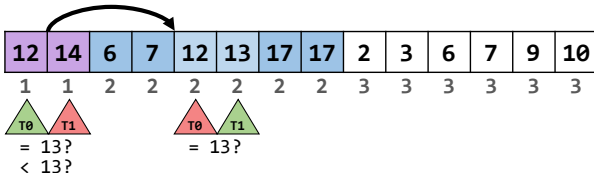


Figure 9: Point lookup of key 13 for EO+KS.

### 3.5 Building the Structures

After describing the layout of our proposed indexing structures, we still have to consider how to build them efficiently on a GPU. While sorting an array of keys can be done quickly using highly-optimized GPU algorithms such as CUB’s DeviceRadixSort [11], the reordering that is required by **EO** is traditionally specified as a recursive algorithm [20], and the **PB** tree also looks at first glance like it has to be built level-by-level. However, we will now show that once we have a sorted copy of the key array, it is possible to implement both the **EO** reordering and the **PB** construction in an embarrassingly parallel way that only requires a single load and a

single store operation per thread, and no cross-thread communication. Just like most GPU algorithms, it works in an out-of-place fashion, placing either the **EO**-reordered array or the **PB** tree into a separate output buffer.

The main idea is to assign a single thread to each slot in the output buffer. The thread then has to figure out which level of the tree it is in (based on its unique TID), and then compute which element from the sorted key array to fetch. This key is then written to the thread’s assigned slot in the output buffer.

When building **AO+PB** for  $n$  keys, the bottom level of the pivot tree has to have  $\lceil \frac{n}{K-1} \rceil$  entries, and each subsequent level is  $\frac{1}{K}$  times the size of the previous one, rounding up if necessary. We store these sizes in a small array, starting with the topmost level, and compute a prefix sum to determine where each level starts in the output buffer. Each thread now locates the rightmost array entry smaller than or equal to its own TID. The position of that entry determines the level we are on, and we can subtract the value at this position from our TID to obtain the position within the level. This prefix sum array only depends on  $n$ , not the key set itself, and can therefore be precomputed on the CPU and copied to fast read-only memory on the GPU. Looking at Figure 8, note that the tree entries in the bottom level are located at positions  $p_i = (K - 1)(i + 1) - 1$ , with the exception of entries that also satisfy  $p_i = K(K - 1)j - 1$  for some integer  $j$ , which will end up on the upper layers. The next level contains all entries indexed by  $p_i = K(K - 1)(i + 1) - 1$  minus all entries that also satisfy  $p_i = K^2(K - 1)j - 1$  for some  $j$ . We can generalize this observation as follows: Given a level  $l$  (where 0 corresponds to the bottommost level) and an intra-level offset  $i$  (starting at 0), the position of the element we have to load from the input buffer is given by

$$p_{l,i} = K^l(K - 1)(1 + i + \lfloor \frac{i}{K-1} \rfloor) - 1.$$

For **EO**, let us first consider the case where the tree is truly complete, i.e., even the leaf level contains the maximum amount of keys. This allows us to compute the offset of level  $l$  directly using the geometric series formula, which yields  $K^l - 1$ . From this, a GPU thread can determine both its level and its position within the level.

In contrast to **AO+PB**, where the newly materialized tree contained only each  $(K - 1)$ -th entry, the **EO** tree obviously includes all entries, which removes the  $(K - 1)$  factor from the equation. Using the same definitions of  $l$  and  $i$  as before, this yields

$$q_{l,i} = K^l(1 + i + \lfloor \frac{i}{K-1} \rfloor) - 1$$

for the load positions for **EO**. This equation can be generalized to regular **EO** trees by making a small adjustment: Consider an **EO** tree where the inner levels are full, but the leaf level only contains a single entry. This entry has to be the leftmost child of the leftmost inner node (by definition of **EO**), and therefore has to be chosen as the smallest key in the dataset (by the search tree property). We can then use the equation above for the inner levels, but we have to correct for the single element that is smaller than all inner-level entries by always adding 1 to  $p_{l,i}$ . More generally, if an entry is located at position  $i$  within inner level  $l$ , there can be at most  $(K - 1)(q_{l,i} + 1)$  entries on the leaf level smaller than that entry. Therefore, we can correct the load position  $q_{l,i}$  of each inner-level entry by adding

$$c_{l,i} = \min(b, (K - 1)(q_{l,i} + 1)),$$

where  $b$  is the actual number of leaf-level entries. These  $b$  leaf-level entries are then placed in the remaining positions, which are given by

$$q_{0,i} = i + \left\lfloor \frac{i}{K-1} \right\rfloor.$$

Figure 10 visualizes the original load positions for the reordered entries from Figure 9.

To the best of our knowledge, we are the first to present a non-recursive build algorithm for **EO** that works for arbitrary input sizes.

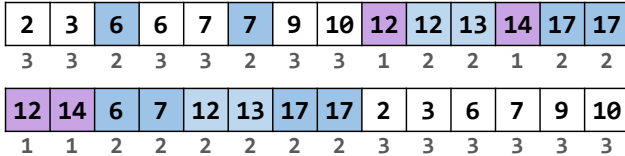


Figure 10: Before and after reordering into  $K$ -ary Eytzinger order. In this example,  $K = 3$  and  $b = 6$ . Note how the bottom-most (white) level is partially interleaved with the top levels.

## 4 Optimizations

While promising, we have seen that the lookup performance of the base methods is not yet fully competitive with more sophisticated index structures. Consequently, we next propose and apply a set of low-level and architecture-driven optimizations to see how far we can push the lightweight methods. Note that while we evaluated and analyzed all meaningful combinations of methods and optimizations, we only show the most interesting and useful combinations, while briefly discussing the remaining possible options.

### 4.1 Limiting Concurrency

As mentioned earlier, the GPU distributes work at the granularity of thread blocks, where by default, a scheduler *dynamically* assigns thread blocks to SMs. The dynamic aspect of this is that the scheduler can schedule multiple thread blocks to a single SM if it deems reasonable, for instance, in order to hide memory stalls or to fully utilize the available compute power.

However, to reduce the load on main memory and the caches, it can be beneficial to purposely limit the amount of threads running at any given time. Hence, in the following, we propose a *static* scheduling strategy, which only spawns a fixed number of thread blocks, namely 128, to match the number of SMs. Then, given **NBTHREAD** as the number of threads per block and **NBLOCK** as the number of blocks, the thread with number **TID** becomes responsible for processing the lookups at positions **TID** +  $i * \text{NBTHREAD} * \text{NBLOCK}$  (for  $i = 0, 1, \dots$ ). This effectively replaces the GPU's dynamic scheduler with a static assignment between lookup tasks and cores.

Apart from the scheduling variant, the number of threads per block **NBTHREAD** likely impacts performance as well, and therefore, we always test multiple block sizes ranging from 128 threads per block (the number of cores per SM) to 1024 threads per block (hardware limit, 8 $\times$  more threads per block than cores per SM).

### 4.2 Cache Pinning Strategies

Across all variants of  $K$ -ary search, the first steps per lookup always access the same few entries and hence should ideally remain in the fastest cache at all times. Unfortunately, by default, these entries

may get evicted and replaced by entries down the search path due to the limited space in the cache. When programming a CPU, there is nothing we could do about this as the L1 cache is automatically managed, but on a GPU, it is possible to actively pin entries by storing them in the up to 100KB large scratch memory, which is carved out of the slightly larger SM-resident 128KB L1 cache. By this, we can effectively exempt top-level entries from being repeatedly flushed from L1 cache during search.

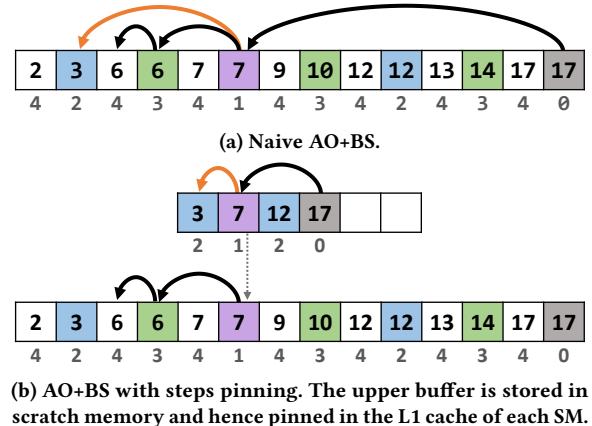


Figure 11: Looking up key 6 with and without cache pinning. Orange arrows denote steps not taken.

**4.2.1 Steps Pinning.** To realize this concept, in the first version called **steps pinning**, we fill the scratch memory with all entries required for performing the first  $M$  steps of the search, where we select the largest  $M$  so that the amount of extracted entries does not exceed the available scratch memory capacity. For **AO+BS**, the subset of entries traversed in the first  $M$  steps of the search is located at positions  $(n-1) - i \frac{S}{2M}$  for  $i = 0, 1, \dots$  (where  $S$  is the initial step size) and is therefore easy to locate and extract. For any **EO** and any **PB** structure, determining the entries is even more straightforward: The entries accessed during the first few steps are those stored in the leftmost slots of the Eytzinger/pivot buffer, and we can copy them to scratch memory as-is.

As an example, consider Figure 11, which shows the data structures and the point lookup of key 6 with and without cache pinning for **AO+BS**. Without cache pinning (Figure 11a), all four steps of the search are carried out in main memory. With cache pinning (Figure 11b) and a hypothetical 6-slot scratch memory region, we can carry out the first  $M = 2$  steps required to find the smallest entry greater than or equal to 6 entirely in scratch memory. Only after that, the search falls back to main memory for the last two steps.

**4.2.2 Full Pinning.** Note that in our example, two slots of the scratch memory were left unused as pinning the next step would require 1 more empty slot. In our second version called **full pinning**, we make use of this unused space by partially caching the entries that would be accessed during step  $M + 1$  of the search. The corresponding changes to the search algorithm are simple: During step  $M + 1$ , we check (via index comparison) if the required entry

is present in scratch memory, and load it from there if possible. Otherwise, we retrieve it from main memory.

For the **EO/PB** indexes, we just store as many of the leftmost slots of the Eytzinger/pivot buffer as we can, even if we cannot fit an entire level.

### 4.3 Reordering Strategies

Even with cache pinning, neighboring threads are still very likely to take different search paths after a few steps. However, if we minimize the absolute difference between lookup keys assigned to neighboring threads, their target positions will probably be close to each other in the sorted array, and therefore their search paths will be mostly identical. An obvious way to achieve this is by globally sorting all lookup keys beforehand. Again, the very positive effect of this can be seen in Figure 1b, where fully sorting all lookups made **AO+BS** perform best among all indexing methods.

**4.3.1 Lookup Reordering.** Unfortunately, globally sorting all lookups also has an unpleasant downside: Most GPU sorting algorithms, including those from CUB, operate out-of-place, which not only introduces additional memory capacity requirements, but also requires efficient allocation and freeing strategies. A reasonable approximation of global sorting is *block-local sorting*, which sorts the key set directly from the threads' registers across all threads in a block. This variant, which we call **lookup reordering** in the following, also runs much faster than sorting globally and only requires a small amount of SM-local scratch memory as a temporary buffer.

The sorting batch size is therefore directly influenced by the number of threads in a block, up to the hardware limit of 1024 threads per block. Increasing the batch size without increasing the block size is still possible by pre-fetching multiple lookup keys into different registers of each thread, and then sorting across multiple registers. This approach is only limited by the number of available registers on the SM. In our experiments, we typically increase the register count as we decrease the block size to keep the sorting batch size constant.

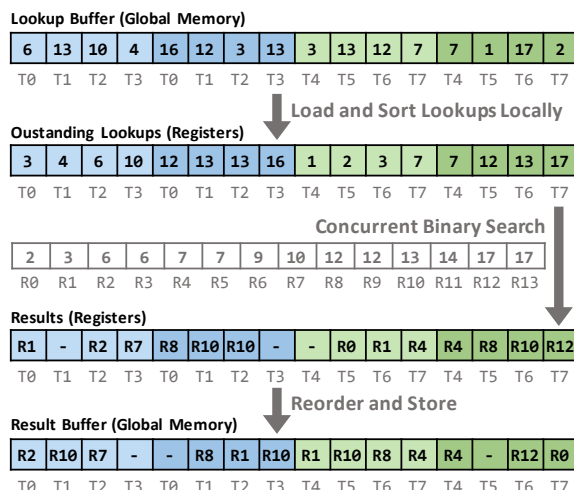


Figure 12: Effect of reordering.

To see how this sequence of pre-fetching and locally sorting works in detail, Figure 12 shows an example for 16 initially unsorted

lookup keys. For simplicity, we assume that each block only has four threads, each of which allocates two registers for lookups. In the first step, we fill the two registers with the keys of the lookup array in the order they were stored. Then, we perform a block-local sort of the keys, followed by two sequential binary searches per thread. The result of each binary search (a row number or a miss) is materialized again in the corresponding registers.

**4.3.2 Double Reordering.** Sadly, lookup reordering introduces an unpleasant side effect: We expect the GPU to write the result of looking up the key at position  $i$  into position  $i$  of the result buffer. If we locally sort the keys, we still have to write the results in the original (unsorted) order, which now consists of almost exclusively random accesses. We can work around this issue by locally applying the inverse of the sort permutation to the results, thus restoring their original order before writing to the result buffer. We call this variant **double reordering** in the following. We can clearly observe the improvement in lookup locality by comparing the resulting row numbers in the lower two buffers in Figure 12.

### 4.4 Memory Layout

Typically, to create a secondary index for a table column, the keys of the column must be copied into a separate memory area while appending a (4B) row ID to each key. Then, the sorting happens on keys and row IDs in pairs. Keys and their associated row IDs can be materialized alternatingly in a single buffer (array-of-structure or **AoS**) or separately in two buffers (structure-of-arrays or **SoA**). Both variants share the same memory footprint, but the choice of layout usually impacts performance, as the amount of memory that must be loaded during lookup processing can differ.

### 4.5 Coarse-granular Pivot Buffer

For small  $K$ , the pivot buffer **PB** can contribute a significant part of the memory footprint. To counteract this, we can materialize only a certain amount of inner levels in the pivot buffer, as shown in Figure 13 for **AO+PB+BS**. Instead of materializing all three inner levels, the example materializes only the first two inner levels, resulting in a smaller pivot buffer of only three entries, but the leaves of the pivot buffer now reference larger four-element partitions. However, if the partitions remain small enough to fit on a cache line, the additional work on the leaf level likely does not cause a significant performance penalty — instead, the memory footprint and the overall performance is improved, as a smaller pivot buffer must be kept and traversed.

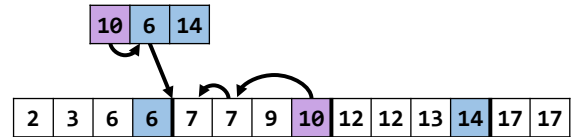


Figure 13: Limiting the number of levels materialized in the pivot buffer to two.

## 5 Pushing the Indexes to their Limits

After having discussed our base indexing methods and the set of possible optimizations, we investigate in the following how the individual optimizations and combinations thereof impact the methods.

## 5.1 Experimental Setup

To quantify our optimization progress, we compare the performance of our proposed lightweight index structures to existing GPU indexes:

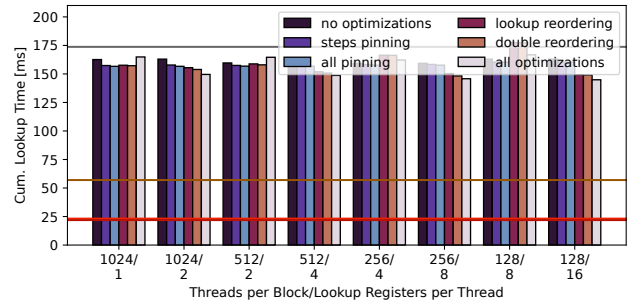
**B+** (brown horizontal line) is the state-of-the-art GPU-resident B+-Tree by Awad et al. [7, 9, 13], without multi-version support. Unfortunately, it only supports 32-bit keys. Lookups are performed with groups of 16 threads, such that determining the next child node can be done concurrently during tree traversal. It uses CUB’s DeviceRadixSort [11] for sorting and bulk-loading the keys. Leaf nodes are bulk-loaded to either 50% or 100% of their maximum capacity.

In terms of hashing schemes (red horizontal line), we include two popular variants of collision resolution: **HT (open)** refers to WarpCore, a state-of-the-art GPU hashtable [18, 19], which implements open addressing with cooperative probing. Each key is assigned to a group of eight threads during inserts or lookups, and each group accesses neighboring slots in the hashtable. This accelerates the task of identifying an empty slot for insertion, or discovering the key to be looked up, while still using the GPU’s cache and load-store units to the maximum extent possible. Since there is no bulk-loading for hashtables, we insert each key separately during the build phase. The target occupancy of the table can be chosen freely, so we always show two variants: 50%, a common choice for CPU-based hash tables, and 80%, which is the authors’ recommendation. **HT (buckets)** is a slightly modified version of SlabHash [5], which uses a chain of linked nodes with 15 slots in each bucket. Similar to **B+**, **HT (buckets)** performs lookups with a group of threads, allowing for efficient traversal of the linked chains, but only supports 32-bit keys as well. Nodes are allocated by a rather sophisticated slab allocator, which had some hard-coded limits we had to remove in order to test larger build sizes. The number of buckets is determined by specifying the desired node occupancy. We test both 100% (each bucket receives an expected number of 15 keys) and 150% (around 22 keys per bucket). Since each of the baselines comes in two variants, we only show the better-performing variant in the introduction and as horizontal lines in the following plots. The final comparison will include all variants. Additionally, we show **AO+BS** (gray horizontal line) as a further reference point.

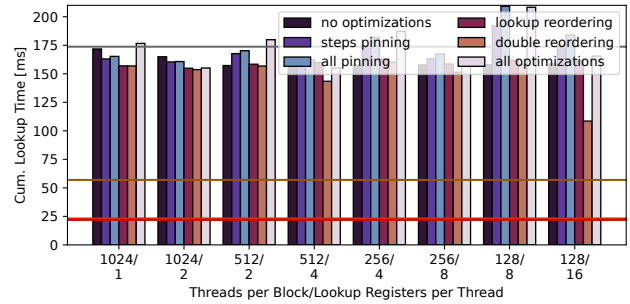
In all following experiments, unless specified otherwise, all data structures are built from a key set of  $2^{28}$  unique and uniformly-drawn 32-bit unsigned integers (**B+** and **HT (buckets)** only support 32-bit keys). A subsequent lookup phase simultaneously probes  $2^{27}$  uniformly-drawn keys from the build set in random order. We assume all data to be GPU-resident and therefore do not include memory allocations or CPU-GPU transfers in our measurements. Further, we only consider workloads where the key set does not change during execution, i.e., no insertions or deletions take place. We compile our implementation using version 12.8 of the CUDA toolchain.

## 5.2 Optimizing AO+BS

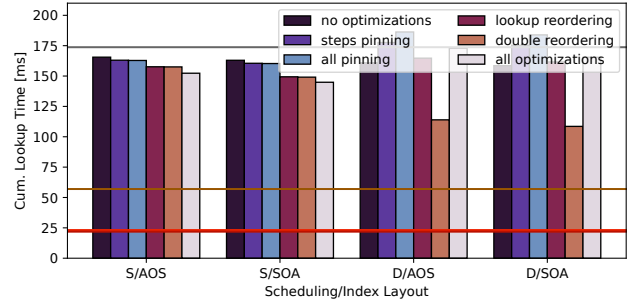
We start with **AO+BS** and see how far we can get even with the most trivial variant of our lightweight indexes. In Figure 14a and Figure 14b, we first focus on the impact of the scheduling strategy and occupancy parameters (threads per block and lookup registers per thread), which likely both have a significant effect on the



(a) Varying the number of threads per block and the lookup registers per thread for static scheduling.



(b) Varying the number of threads per block and the lookup registers per thread for dynamic scheduling.



(c) Varying the scheduling strategy and the memory layout.

Figure 14: Impact of optimizations for AO+BS.

method, while testing the impact of the cache pinning and local reordering optimizations. In Figure 14c, we then fix the occupancy parameters to 128/16 and vary the memory layout instead.

Let us focus first on static scheduling in Figure 14a. We vary two occupancy parameters that are directly connected to each other: (1) The number of threads per block from 1024 down to 128, which equals the number of cores per SM. (2) The number of lookup registers that we reserve for each thread, where we keep the total number of registers per block constant at either 1024 or 2048. From a distance, we can already observe that the application of both cache pinning and lookup reordering can significantly improve the performance of **AO+BS**, where the double variant beats the respective single variant. However, we can also observe that the effectiveness

of these optimizations depends on the occupancy parameters. This becomes apparent when sorting: Increasing the number of lookup registers per block automatically increases the sorting batch size. Sorting becomes more expensive, especially when there are fewer threads involved, but the lookup locality benefits from larger sorted batches, since the expected difference (and therefore, their search path divergence) between neighboring keys decreases. For dynamic scheduling in Figure 14b, the lookup times are more fluctuating because many factors can influence the GPU’s scheduling choices. Dynamic scheduling is mostly worse than static scheduling, except for a few significant outliers. This is especially pronounced with **steps pinning** and **full pinning**, which actually increase the total execution time. A possible explanation for this originates from the fact that each newly scheduled thread block has to re-fill the scratch memory before execution, which takes longer when there are fewer threads per block, and eventually overshadows the potential benefits of pinning. In contrast, reordering with a small number of threads performs better when using dynamic scheduling, because sorting only uses few SM resources, allowing multiple blocks to sort their lookups concurrently on the same SM.

When focusing on the memory layout in Figure 14c, we can see very little impact under both static and dynamic scheduling. **SoA** layout shows a slightly better performance than **AoS**, which implies that binary search benefits from a denser storage layout.

Overall, by applying our optimizations cache pinning and local reordering, we are already able to improve the performance of the base **AO+BS** under 128 threads per block for 16 registers per thread. Nevertheless, the next best baseline **B+** is still around 1.75× faster, so we have not reached our goal yet.

### 5.3 Optimizing EO+BS

Hence, we next test how the variant using the Eytzinger order **EO+BS** reacts to the optimizations. Figure 15 shows its lookup performance for dynamic scheduling. Note that due to space constraints, we omit the static scheduling and the memory layout graph, as the observations are very similar to the one made for **AO+BS**.

We can see that **EO+BS** does not benefit from the cache pinning optimization, as the layout is already very cache-optimized. Simultaneously, the Eytzinger layout also offers better locality for slightly-diverging lookup paths, which further improves the effectiveness of reordering.

Consequently, **EO+BS** manages to further improve over the previously studied best configuration of **AO+BS** and is now only around 1.35× behind the next best baseline **B+**, making it clearly the superior variant for point lookups. Note that we will study the impact on range lookups in Section 5.7.

### 5.4 Optimizing AO+PB+BS

Next, let us see how the variant materializing the pivots of the search part, namely **AO+PB+BS**, can be optimized. Here, we focus primarily on how many levels of the search tree should actually be materialized in the pivot buffer. In particular, we are interested in identifying whether a smaller search tree with a smaller memory footprint also yields decent performance.

Figure 16 shows the results, where we evaluate pivot buffers covering 10, 20, 24, and 27 levels. We can see that even with the increase in memory footprint, a larger pivot buffer of up to 24 levels improves the lookup time significantly and should indeed be used if the space

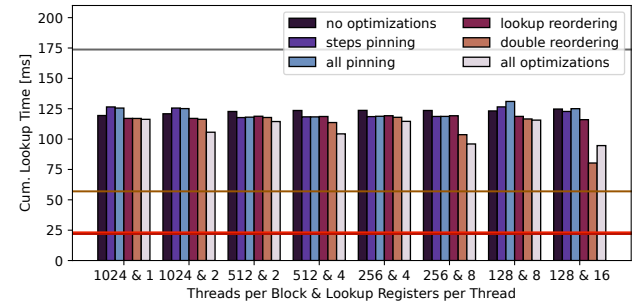


Figure 15: Impact of optimizations for EO+BS.

constraints allow for it. However, we can also see that materializing the full search tree of 27 levels is not beneficial but deteriorates the performance. The reason for this is that performing binary search on the final  $2^4 = 16$  candidate elements can be done very efficiently on the full array, since for **AoS** layout, these elements exactly fit on a single cache line. For **SoA** layout, the performance is slightly worse, as two cache lines must be loaded for the final binary search. Also note that for 24 levels, which showed the best performance, the additional pivot buffer has a size of only 64MB, which makes a negligible 3% of the total memory footprint and is hence certainly worth it.

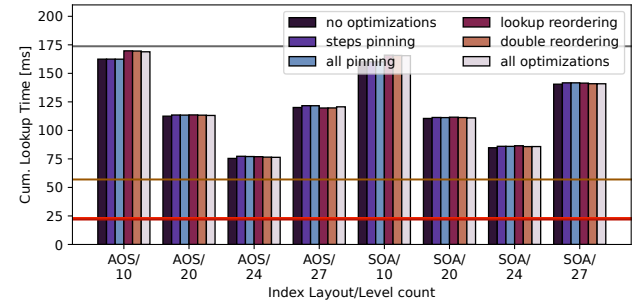


Figure 16: Impact of optimizations for AO+PB+BS.

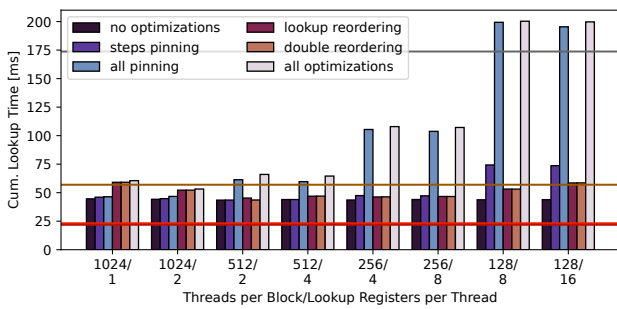
In total, the optimized version of **AO+PB+BS** clearly further improves the performance over **EO+BS** and almost reaches the **B+** baseline, which only remains 1.25× faster.

### 5.5 Optimizing EO+KS

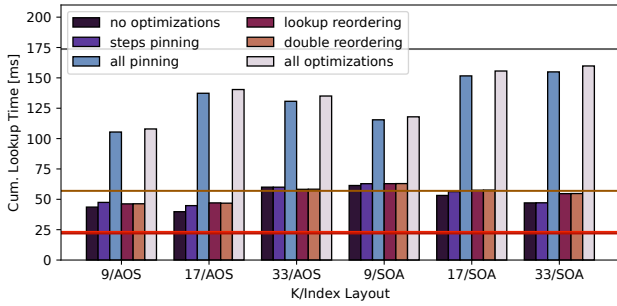
Let us now see whether optimizing the  $K$ -ary search variants changes the picture. We start with **EO+KS** having again a minimal memory footprint. Figure 17 shows the results, where in Figure 17a, we first vary the occupancy parameters for dynamic scheduling as usual. Then, we use the best obtained configuration and vary the fan-out  $K$  as well as the memory layout in Figure 17b.

First, we can see that pinning completely deteriorates the lookup performance. The reason for this is likely not the pinning itself, but a side-effect of pinning: Dynamic scheduling tries to schedule multiple thread blocks onto the same SM if the SM can provide sufficient resources (registers, scratch memory) for all of them. However, **full pinning** reserves *all* scratch memory, and therefore,

the block scheduler cannot schedule two thread blocks onto the same SM. This seems counter-intuitive because the pinned data is the same for every block, but of course, the scheduler does not know this, and the CUDA programming model does not allow sharing scratch memory across blocks. Second, reordering does not provide a visible benefit. This is to be expected since lookups are performed by groups of threads, and threads within the group always take the same lookup path anyway, so the impact of reordering is limited to improving inter-group locality, but still incurs the overhead of performing the block-local sort. Third, the choice between **AoS** and **SoA** layout is interlinked with the choice of  $K$ . Large node sizes prefer **SoA** layout, while smaller node sizes prefer the opposite. When accounting for the appropriate layout, the execution times are similar and leave the programmer free reign over the node width / tree depth tradeoff.



(a) Varying the number of threads per block and the lookup registers per thread for dynamic scheduling.



(b) Varying  $K$  and the memory layout.

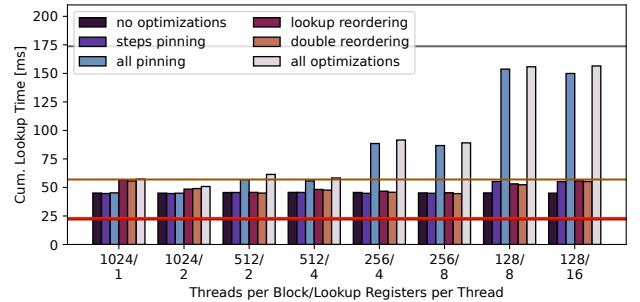
Figure 17: Impact of optimizations for EO+KS.

Overall, **EO+KS** is the first baseline that actually beats **B+** by being around 1.6× faster. This is especially impressive since this indexing schemes does not use any auxiliary data structure, but just the full array. Also, the now next best baseline **HT** is only 1.6× away as well, however, having a significantly higher memory footprint.

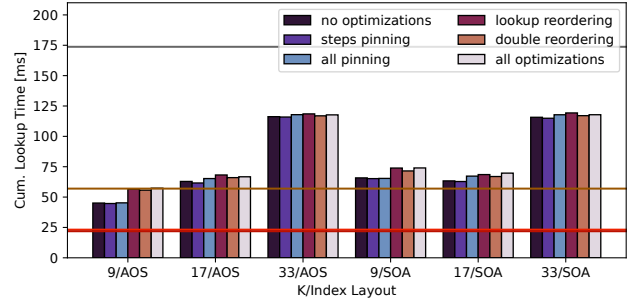
## 5.6 Optimizing AO+PB+KS

Finally, let us look at the impact of the optimizations for **AO+PB+KS** as shown in Figure 18. As Figure 18a shows, for dynamic scheduling, he behavior closely follows **EO+KS**, although less exaggerated, and similar reasoning applies here. Figure 18b shows the impact of the fan-out  $K$  and the index layout for occupancy configuration

1024/1, which is quite different from the **EO+KS** results. With a larger thread count, the pinning optimizations do not have a significant negative impact. However, we can also see that **AoS** layout performs better than **SoA** layout, and a larger fan-out negatively impacts throughput.



(a) Varying the number of threads per block and the lookup registers per thread for dynamic scheduling.



(b) Varying  $K$  and the memory layout.

Figure 18: Impact of optimizations for AO+PB+KS.

As summary, we can observe that the best configuration of **AO+PB+KS** behaves as good as **EO+KS** for point lookups, but also not better. However, as this variant keeps the sorted array, it might still be an interesting alternative if fast range-lookups are required.

## 5.7 Optimizing for Range Lookups

Consequently, let us now see how the methods can perform range lookups efficiently as well, which include a range scan part after the traversal.

As described in Section 3.4, for the variants performing **KS**, the range scan is parallelized naturally across  $K - 1$  threads. However, for the methods using **BS** which perform a single-threaded traversal, the subsequent range scan can still be performed by multiple threads scanning adjacent entries. Intuitively, this is only beneficial if a sufficiently large number of entries has to be traversed, since mobilizing the additional threads incurs some amount of overhead. We settled on the following heuristic, which is applicable to **AO+(PB)+BS**: In a group of 32 adjacent threads, we perform 32 lookups in total, where each thread individually performs the search for its lower bound in the pivot buffer, and then starts traversing the ascending key array for up to 32 elements, or less if it arrives at the end of the range. Afterwards, the threads communicate to

compute which ones did not finish their scan. Then, sequentially for each unfinished scan, the position of the last scanned entry is scattered across all 32 threads, and they continue the scan together. The threshold of 32 ensures that the switch from single-threaded to multi-threaded traversal never dominates the execution time.

We can apply a similar strategy to **EO+BS**: If we find at least three qualifying entries within a single Eytzinger level, the amount of qualifying entries strictly increases on the next level, because the three entries have at least four qualifying child entries between them (and this argument can be applied inductively). Therefore, once a thread traverses more than 32 entries in a single level, all subsequent levels will be scanned using all 32 threads.

Figure 19 shows the results for performing  $2^{16}$  range lookups that each scan a fixed-size range starting at an offset uniformly drawn that yields  $2^6$  respectively  $2^{14}$  expected hits. We evaluate both single-threaded and multi-threaded range scans and re-evaluate the choice of memory layout, as range queries are typically very sensitive to it.

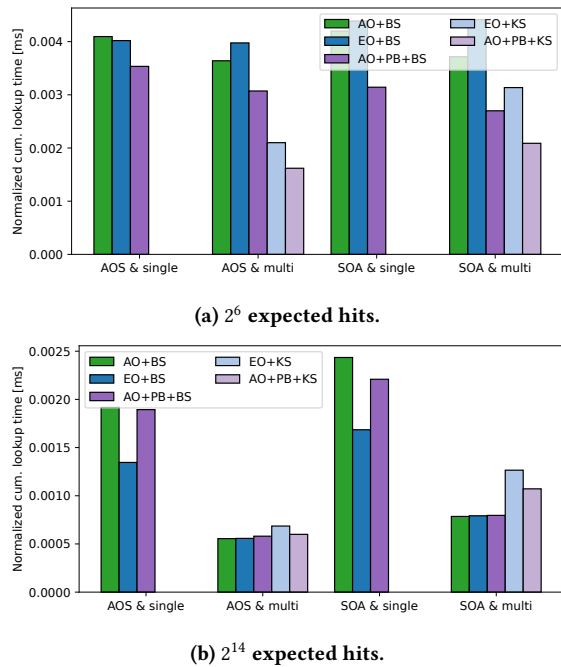


**Figure 19: Comparing single-threaded with multi-threaded range scan using both memory layouts. Note that the **KS** variants always perform a multi-threaded scan.**

The results in Figure 19 confirm our expectations: Switching to the multi-threaded strategy is always beneficial, regardless of the base index we apply it to, even if the size of the range lookup barely exceeds the switching threshold. Regarding layout, this experiment mirrors the previous result that the **KS** variants prefer **AoS** over **SoA**, but now, all other variants also experience a slight performance increase when using **AoS** layout. This can be explained by noticing that a range lookup has to access the row IDs for *all* qualifying keys, not just one. With **AoS** layout, the row IDs are stored immediately next to the keys, and therefore already in L1 cache when they are accessed.

## 6 Scaling Experiments

After having optimized all lightweight indexes as much as possible, let us perform a final comparison with the baseline methods. We compare the point lookup performance of our optimized methods (Figure 20a) against the baselines and also report a composite metric called *throughput per memory footprint* to see how the individual methods “pay” for their performance with an increased memory footprint, e.g., by building auxiliary data structures or by performing over-allocation (Figure 20b). Further, we compare the range lookup performance (Figure 22) and finally the build time and memory footprint (Figure 21) of all indexes.

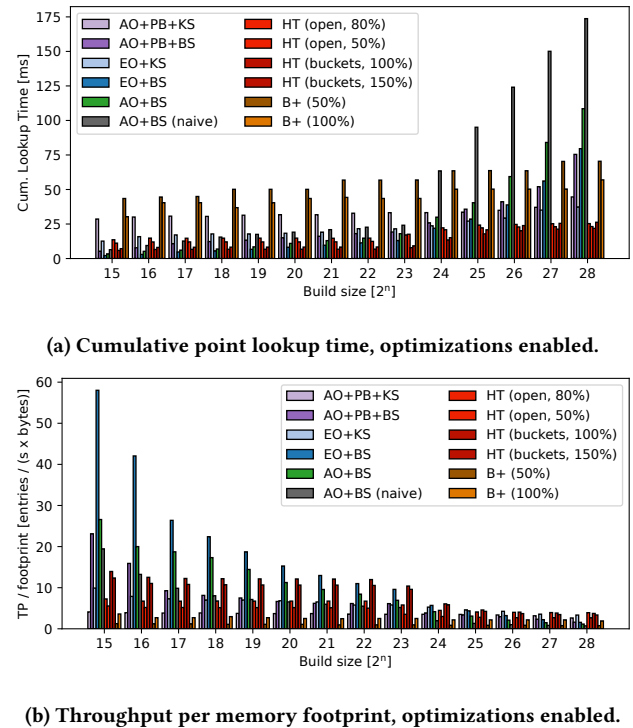


**Figure 20: Point lookup comparison of our optimized lightweight indexes with the baseline indexes.**

In terms of point lookup performance, the results yield several insights: First, our initial goal of supercharging **AO+BS** resulted in massive speedups over the naive variant once the dataset exceeds the size of the L2 cache, sometimes achieving speedups of more than 200%. A similar effect is observable for the other index structures. Second, for smaller datasets, **EO+BS** outperforms every other index, and can remain competitive with the GPU hash tables up to an input size of  $2^{24}$ . In fact, we motivated this paper by stating the surprisingly good performance of **AO+BS**, and **EO+BS** surpassed even that. Third, for small datasets, the **KS** variants initially perform poorly, but their absolute lookup time barely increases as the size of the dataset grows, so that they outperform everything but the hash tables once we hit  $2^{26}$  elements. The choice between **AO** and **EO** does not make a large difference at this point. Fourth, **AO+PB+BS** outperforms its non-**PB** competitor for large datasets, despite its larger memory footprint.

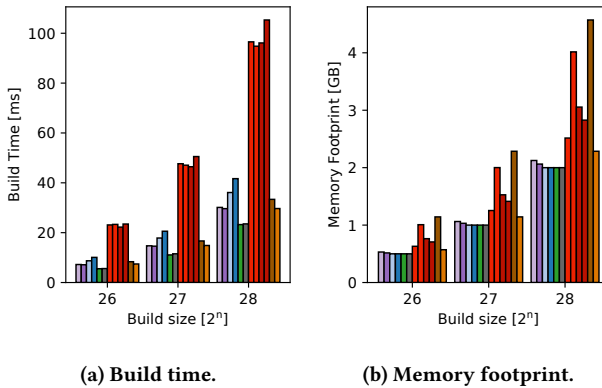


Figure 21: Build time and memory footprint.

In terms of build time, we can see our lightweight indexes are competitive with **B+** and clearly outperform the **HT** variants. Requiring at most around 50ms to construct an index with  $2^{28}$  entries shows that fully rebuilding our indexes in order to handle a batch of updates in read-mostly workload can be a viable option. Regarding memory consumption, as intended, the lightweight variants show the smallest footprint of all methods, even for the variants using **PB**.

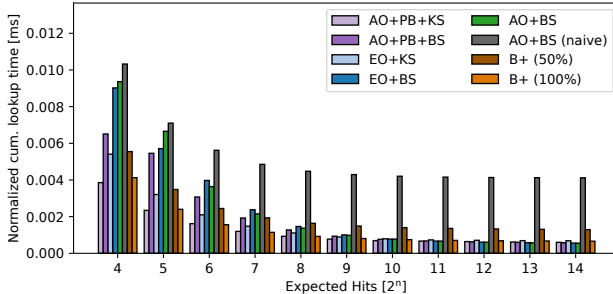


Figure 22: Range lookup comparison of our fully optimized lightweight indexes with **B+**.

Finally, regarding range lookups, we can observe **AO+PB+KS** yields the best performance of all lightweight methods and stays on par with the densely populated **B+**. Although the Eytzinger variant **EO+KS** performs a bit worse as it must split scans across Eytzinger levels, it is nice to see that its distance to **AO+PB+KS** is rather small and quickly decreases with an increase in range.

## 6.1 Decision Tree

This leaves us with the following “decision tree” for selecting the perfect lightweight index structure: If ascending order is not a strict requirement, or if we need to ensure the smallest possible memory footprint, *always* use Eytzinger search. If the input size exceeds L2 size, a larger  $K$  (in our experiments,  $K = 9$ ) as well as multi-threaded lookups improve performance. If ascending order is absolutely required, or the workload consists of many small range lookups, or we need short rebuild times, use the optimized binary search, and switch to a **PB** approach once the input becomes too large. Further, if your workload includes range lookups, always

choose **AoS** layout over **SoA**. Also, never use **PB** in combination with **BS**.

## 7 Related Work

In recent years, several CPU index structures have been ported successfully to GPUs.

This includes hash tables [2, 3, 5, 16, 18, 21, 27], from which we selected our baselines **HT (open)** and **HT (buckets)**, as well as comparison based structures like our baseline **B+**. Further, radix trees [1] have been proposed, where however, no public implementation is currently available. There also exist GPU-resident spatial indexes such as R-Trees [24, 26] and GPU permutation indexes [23], which however, target different use cases than our indexes.

In terms of index structures specifically tailored towards the read-only scenario, which we primarily target in this work, there exist two GPU-resident learned indexes [28] and [22], which typically tend to come with a high lookup performance in combination with a low memory footprint. While the implementation of the former is not available, the latter is unfortunately not a full-fledged GPU-index, as it utilizes the CPU-variant of the PGM learned index [12] for construction, and then moves the data structure over to GPU-memory to perform the lookups in parallel. A similar strategy has been applied in [10] proposing a hash table performing perfect hashing, which offers minimal lookup time at the cost of a more expensive build phase. While the build phase can be run entirely on the GPU, the lookup procedure requires pre-partitioning on the CPU to work correctly. As we do not consider these indexes as full-fledged GPU data structures that perform all operations on the device itself like our indexes, but rather as GPU-accelerated CPU-indexes, we did not include them in the current evaluation.

## 8 Conclusion

In this work, we pushed the concept of minimalist lightweight indexing in form of binary search and related variants to its limits. We showed that for both point and range lookups, our carefully optimized lightweight indexes manage to clearly outperform a densely-packed **B+-tree** by a factor of  $1.6\times$ , while having a minimal or close to minimal memory footprint. Further, our lightweight indexes are only  $1.6\times$  behind the the very best hash table variant while having a significantly lower build time, memory footprint, as well as range lookup support. By this, we showed that minimalist lightweight indexing on GPUs is a practical alternative to complex state-of-the-art GPU-resident index structures in read-only or read-mostly environments.

## References

- [1] Md. Maksudul Alam, Srikanth B. Yoginath, and Kalyan S. Perumalla. 2016. Performance of Point and Range Queries for In-memory Databases Using Radix Trees on GPUs. In *18th IEEE International Conference on High Performance Computing and Communications; 14th IEEE International Conference on Smart City; 2nd IEEE International Conference on Data Science and Systems, HPCC/SmartCity/DSS 2016, Sydney, Australia, December 12–14, 2016*, Jinjun Chen and Laurence T. Yang (Eds.). IEEE Computer Society, 1493–1500. <https://doi.org/10.1109/HPCC-SmartCity-DSS.2016.0212>
- [2] Dan A. Alcantara, Andrei Sharf, Fatemeh Abbasinejad, Shubhabrata Sengupta, Michael Mitzenmacher, John D. Owens, and Nina Amenta. 2009. Real-time parallel hashing on the GPU. *ACM Trans. Graph.* 28, 5 (2009), 154. <https://doi.org/10.1145/1618452.1618500>
- [3] Dan A. Alcantara, Vasily Volkov, Shubhabrata Sengupta, Michael Mitzenmacher, John D. Owens, and Nina Amenta. 2012. Chapter 4 - Building an Efficient Hash Table on the GPU. In *GPU Computing Gems Jade Edition*, Wen mei W. Hwu (Ed.).

Morgan Kaufmann, Boston, 39–53. <https://doi.org/10.1016/B978-0-12-385963-1.00004-6>

[4] Saman Ashkiani, Martin Farach-Colton, and John D. Owens. 2018. A Dynamic Hash Table for the GPU. In *2018 IEEE International Parallel and Distributed Processing Symposium, IPDPS 2018, Vancouver, BC, Canada, May 21–25, 2018*. IEEE Computer Society, 419–429. <https://doi.org/10.1109/IPDPS.2018.00052>

[5] Saman Ashkiani, Martin Farach-Colton, and John D. Owens. 2018. A Dynamic Hash Table for the GPU. In *2018 IEEE International Parallel and Distributed Processing Symposium, IPDPS 2018, Vancouver, BC, Canada, May 21–25, 2018*. IEEE Computer Society, 419–429. <https://doi.org/10.1109/IPDPS.2018.00052>

[6] Muhammad A. Awad, Saman Ashkiani, Rob Johnson, Martin Farach-Colton, and John D. Owens. 2019. Engineering a high-performance GPU B-Tree. In *Proceedings of the 24th ACM SIGPLAN Symposium on Principles and Practice of Parallel Programming, PPoPP 2019, Washington, DC, USA, February 16–20, 2019*, Jeffrey K. Hollingsworth and Idit Keidar (Eds.). ACM, 145–157. <https://doi.org/10.1145/3293883.3295706>

[7] Muhammad A. Awad, Saman Ashkiani, Rob Johnson, Martin Farach-Colton, and John D. Owens. 2019. Engineering a high-performance GPU B-Tree. In *Proceedings of the 24th ACM SIGPLAN Symposium on Principles and Practice of Parallel Programming, PPoPP 2019, Washington, DC, USA, February 16–20, 2019*, Jeffrey K. Hollingsworth and Idit Keidar (Eds.). ACM, 145–157. <https://doi.org/10.1145/3293883.3295706>

[8] Muhammad A. Awad, Serban D. Porumbescu, and John D. Owens. 2022. A GPU Multiversion B-Tree. In *Proceedings of the International Conference on Parallel Architectures and Compilation Techniques, PACT 2022, Chicago, Illinois, October 8–12, 2022*, Andreas Klöckner and José Moreira (Eds.). ACM, 481–493. <https://doi.org/10.1145/3559009.3569681>

[9] Muhammad A. Awad, Serban D. Porumbescu, and John D. Owens. 2022. A GPU Multiversion B-Tree. In *Proceedings of the International Conference on Parallel Architectures and Compilation Techniques, PACT 2022, Chicago, Illinois, October 8–12, 2022*, Andreas Klöckner and José Moreira (Eds.). ACM, 481–493. <https://doi.org/10.1145/3559009.3569681>

[10] Jiaping Cao, Le Xu, Man Lung Yiu, Jianbin Qin, and Bo Tang. 2025. GPH: An Efficient and Effective Perfect Hashing Scheme for GPU Architectures. *Proc. ACM Manag. Data* 3, 3 (2025), 165:1–165:26. <https://doi.org/10.1145/3725406>

[11] NVIDIA Corporation. 2022. CUB. <https://nvlabs.github.io/cub/> Accessed on February 27th, 2023.

[12] Paolo Ferragina and Giorgio Vinciguerra. 2020. The PGM-index: a fully-dynamic compressed learned index with provable worst-case bounds. *Proc. VLDB Endow.* 13, 8 (2020), 1162–1175. <https://doi.org/10.14778/3389133.3389135>

[13] Owens Research Group. 2021. MVGpuBTree: Multi-Value GPU B-Tree. <https://github.com/owensgroup/MVGpuBTree> Accessed: February 27, 2023.

[14] Justus Henneberg and Felix Schuhknecht. 2023. RTIndex: Exploiting Hardware-Accelerated GPU Raytracing for Database Indexing. *Proc. VLDB Endow.* 16, 13 (2023), 4268–4281. <https://www.vldb.org/pvldb/vol16/p4268-schuhknecht.pdf>

[15] Justus Henneberg, Felix Schuhknecht, Rosina Kharal, and Trevor Brown. 2025. More Bang For Your Buck(et): Fast and Space-efficient Hardware-accelerated Coarse-granular Indexing on GPUs. In *41th IEEE International Conference on Data Engineering, ICDE 2025, Hong Kong SAR, China, May 19–23, 2025*. IEEE.

[16] Daniel Jünger, Christian Hundt, and Bertil Schmidt. 2018. WarpDrive: Massively Parallel Hashing on Multi-GPU Nodes. In *2018 IEEE International Parallel and Distributed Processing Symposium, IPDPS 2018, Vancouver, BC, Canada, May 21–25, 2018*. IEEE Computer Society, 441–450. <https://doi.org/10.1109/IPDPS.2018.00054>

[17] Daniel Jünger, Robin Kobus, André Müller, Christian Hundt, Kai Xu, Weiguo Liu, and Bertil Schmidt. 2020. WarpCore: A Library for fast Hash Tables on GPUs. In *27th IEEE International Conference on High Performance Computing, Data, and Analytics, HiPC 2020, Pune, India, December 16–19, 2020*. IEEE, 11–20. <https://doi.org/10.1109/HIPC50609.2020.00015>

[18] Daniel Jünger, Robin Kobus, André Müller, Christian Hundt, Kai Xu, Weiguo Liu, and Bertil Schmidt. 2020. WarpCore: A Library for fast Hash Tables on GPUs. In *27th IEEE International Conference on High Performance Computing, Data, and Analytics, HiPC 2020, Pune, India, December 16–19, 2020*. IEEE, 11–20. <https://doi.org/10.1109/HIPC50609.2020.00015>

[19] Daniel Jünger. 2022. warpcore. <https://github.com/sleepyjack/warpcore> Accessed: February 27, 2023.

[20] Paul-Virak Khuong and Pat Morin. 2017. Array Layouts for Comparison-Based Searching. *ACM J. Exp. Algorithmics* 22 (2017). <https://doi.org/10.1145/3053370>

[21] Yuchen Li, Qiwei Zhu, Zheng Lyu, Zhongdong Huang, and Jianling Sun. 2021. DyCuckoo: Dynamic Hash Tables on GPUs. In *37th IEEE International Conference on Data Engineering, ICDE 2021, Chania, Greece, April 19–22, 2021*. IEEE, 744–755. <https://doi.org/10.1109/ICDE51399.2021.00070>

[22] Jiesong Liu, Feng Zhang, Lv Lu, Chang Qi, Xiaoguang Guo, Dong Deng, Guoliang Li, Huanchen Zhang, Jidong Zhai, Hechen Zhang, Yuxing Chen, Anqun Pan, and Xiaoyong Du. 2024. G-Learned Index: Enabling Efficient Learned Index on GPU. *IEEE Trans. Parallel Distributed Syst.* 35, 6 (2024), 795–812. <https://doi.org/10.1109/TPDS.2024.3381214>

[23] Mariela Lopresti, Fabiana Piccoli, and Nora Reyes. 2021. GPU Permutation Index: Good Trade-Off Between Efficiency and Results Quality. In *Computer Science - CACIC 2021 - 27th Argentine Congress, CACIC 2021, Salta, Argentina, October 4–8, 2021, Revised Selected Papers (Communications in Computer and Information Science, Vol. 1584)*, Patricia Pesado and Gustavo Gil (Eds.). Springer, 183–200. [https://doi.org/10.1007/978-3-031-05903-2\\_13](https://doi.org/10.1007/978-3-031-05903-2_13)

[24] Sushil K. Prasad, Michael McDermott, Xi He, and Satish Puri. 2015. GPU-based Parallel R-tree Construction and Querying. In *2015 IEEE International Parallel and Distributed Processing Symposium Workshop, IPDPSW 2015, Hyderabad, India, May 25–29, 2015*. IEEE Computer Society, 618–627. <https://doi.org/10.1109/IPDPSW.2015.127>

[25] Jun Rao and Kenneth A. Ross. 1999. Cache Conscious Indexing for Decision-Support in Main Memory. In *VLDB'99, Proceedings of 25th International Conference on Very Large Data Bases, September 7–10, 1999, Edinburgh, Scotland, UK*, Malcolm P. Atkinson, Maria E. Orlowska, Patrick Valduriez, Stanley B. Zdonik, and Michael L. Brodie (Eds.). Morgan Kaufmann, 78–89. <http://www.vldb.org/conf/1999/P7.pdf>

[26] Simin You, Jianting Zhang, and Le Gruenwald. 2013. Parallel spatial query processing on GPUs using R-trees. In *Proceedings of the 2nd ACM SIGSPATIAL International Workshop on Analytics for Big Geospatial Data, BigSpatial@SIGSPATIAL 2013, Nov 4th, 2013, Orlando, FL, USA*, Varun Chandola and Ranga Raju Vatsavai (Eds.). ACM, 23–31. <https://doi.org/10.1145/2534921.2534949>

[27] Kai Zhang, Kaibo Wang, Yuan Yuan, Lei Guo, Rubao Lee, and Xiaodong Zhang. 2015. Mega-KV: A Case for GPUs to Maximize the Throughput of In-Memory Key-Value Stores. *Proc. VLDB Endow.* 8, 11 (2015), 1226–1237. <https://doi.org/10.14778/2809974.2809984>

[28] Kun Zhong, Yong Zhang, Yu Chen, Chao Li, and Chunxiao Xing. 2022. Learned Index on GPU. In *38th IEEE International Conference on Data Engineering Workshops, ICDE Workshops 2022, Kuala Lumpur, Malaysia, May 9, 2022*. IEEE, 117–122. <https://doi.org/10.1109/ICDEW55742.2022.00024>